Ceramics International 42 (2016) 18289–18295

Contents lists available at ScienceDirect

Ceramics International

journal homepage: www.elsevier.com/locate/ceramint

Nanostructured Cerium-doped ZnO thin film – A breath sensor

Arockia Jayalatha Kulandaisamy [a,b], Vignesh Elavalagan [a,b], Prabakaran Shankar [a,b], Ganesh Kumar Mani [a,b,c], K. Jayanth Babu [a,b], John Bosco Balaguru Rayappan [a,b,*]

[a] Nano Sensors Lab @ Centre for Nano Technology & Advanced Biomaterials (CeNTAB), SASTRA University, Thanjavur, 613401 India
[b] School of Electrical & Electronics Engineering (SEEE), SASTRA University, Thanjavur, 613401 India
[c] Micro/Nano Technology Center, Tokai University, Japan

ARTICLE INFO

Article history:
Received 13 July 2016
Received in revised form
18 August 2016
Accepted 25 August 2016
Available online 26 August 2016

Keywords:
ZnO
Cerium doping
Acetone
Ethanolamine
Diabetes
Carcinoma
Gas sensor

ABSTRACT

Breath analysis has emerged as one of the accurate diagnostic techniques, which can be used to correlate disease conditions with the abnormal concentrations of certain biomarkers present in the exhaled breath. In this background, thin film based chemi-resistive Cerium-doped ZnO sensors were developed for detecting acetone and ethanolamine, which are the notable biomarkers of diabetes mellitus and carcinoma respectively. Ce-doped ZnO thin films were deposited on glass substrates using spray pyrolysis technique. X-ray diffraction patterns confirmed the formation of Ce-doped ZnO thin films with polycrystalline hexagonal wurtzite structure. Scanning electron micrographs and optical absorption spectra of Ce-doped ZnO thin films revealed the decrease in average grain size and increase in band gap respectively with an increase in Ce-dopant concentration. ZnO films with 0.004 and 0.008 M of Ce-dopant concentrations showed a better room temperature sensing response towards acetone and ethanolamine respectively. Highly selective nature of the developed sensing elements towards acetone and ethanolamine with swift response and recovery times can be considered as a non-invasive and cost effective method for the detection of diseases like diabetes mellitus and carcinoma.

1. Introduction

The detection of Volatile Organic Compounds (VOCs) in human breath, sweat and urine has been identified as a new frontier in disease diagnostic methods [1]. Specifically, the presence of VOCs like acetone, acetaldehyde, ammonia, ethanolamine, etc., in human excretes acts as the fingerprints for diseases like diabetes mellitus, chronic obstructive pulmonary disease, halitosis, kidney malfunction and lung cancer [1–3]. In 1857, Petters observed the presence of acetone odour in the exhaled breath of patients suffering from diabetes mellitus [4,5]. Traces of acetone in exhaled breath is due to the incomplete utilization of glucose in blood, which leads to the production of higher levels of acetone say greater than 1.8 ppm for diabetic patients while less than 0.9 ppm for healthy people [6]. Similar to acetone, ethanolamine is also an important biomarker to detect liver disorder. Dent and Walshe [7] reported the presence of abnormal concentration of ethanolamine in urine of a patient having amino acid metabolism disorder in liver, which leads to primary carcinoma.

Till today, detection of these types of biomarkers is performed using diagnosis techniques like Gas Chromatography (GC), Mass Spectrometer (MS), Fourier Transform Infrared Spectrometer (FTIR), Nondispersive Infrared Spectroscopy (NDIR), Nondispersive Isotope-selective Infrared Spectroscopy (NDIRS), Chemiluminescence, Electrochemical, Colorimetric, Surface Acoustic Wave (SAW), Selected Ion Flow Tube (SIFT) methods [2]. Even though these techniques show rapid and good selective detection of target vapours or aromas, they are limited due to their size, cost and time consuming processing steps. To overcome these limitations, metal oxide based chemiresistive breath sensors have been developed owing to their advantages like miniaturized size, portability, highly sensitive, non-invasive and cost effectiveness [6].

In the recent past, ZnO has been extensively studied by many researchers owing to its potential applications in various fields and particularly in fabricating sensor devices [8–19]. To enhance its sensing performance, significant efforts have been made like doping of metal oxides or metals [20–24]. Doping has been an important and effective technique to tune the structural and morphological properties of ZnO for desired applications [25,26]. Reduced graphene oxide doped SnO_2 [27], metal [28] and organic elements doped ZnO [29] were investigated to improve the acetone sensing characteristics by enhancing the sorption process of acetone vapour without modulating the activation energy of the sensing surface. Among various doping elements, cerium is found to be an interesting element due to its key features like availability

* Corresponding author at: School of Electrical & Electronics Engineering (SEEE), SASTRA University, Thanjavur 613401, India.
E-mail address: rjbosco@ece.sastra.edu (J.B.B. Rayappan).

http://dx.doi.org/10.1016/j.ceramint.2016.08.156
0272-8842/

of 4f orbital, ionic bonding between Ce–O [30], chemically stable nature, redox coupling of Ce^{3+}/Ce^{4+}, easy formation of labile oxygen vacancies with relatively high mobility of bulk oxygen species [31] and control over modifying the morphological properties of the host. Ce-dopants favoured better chemical interaction with acetone molecules for enhanced response [32–35]. Ge et al. [35] observed the influence of Ce-dopants in the sorption process during gas-solid interaction. To the best of our knowledge, very few reports are available explaining the microstructural and sensing mechanism of Ce-doped ZnO nanostructured films prepared using spray pyrolysis technique. Hence, in the present study, the effect of cerium-dopants on the acetone and ethanolamine sensing characteristics of ZnO in the context of developing non-invasive disease diagnostic tool for detecting diabetes mellitus and carcinoma has been investigated and reported.

2. Materials and methods

2.1. Film deposition and formation

Undoped and Ce-doped ZnO thin films were deposited on glass substrates using spray pyrolysis technique (HOLMARC HO-TH-04, Kerala, India). 0.1 M zinc acetate dihydrate (Sigma Aldrich, 99% purity) and different molar concentrations (0.002 M, 0.004 M, 0.006 M, 0.008 M to 0.01 M) of cerium (III) acetate hydrate (Sigma Aldrich, 99% purity) were dissolved in 50 mL of deionized water to prepare the precursor solution. Glass substrates were ultrasonically cleaned using acetone, isopropanol and deionized water. The obtained precursor solutions with desired concentrations were deposited on preheated glass substrates at 523 K and the optimized deposition parameters are given in Table 1. The sprayed aqueous solution was thermally decomposed on the hot substrate in-turn resulted in the formation of ZnO and Ce-doped ZnO thin films. The deposited undoped and Ce-doped ZnO samples were annealed at 673 K for 1 h to remove the residues and to enhance the crystallinity and stability of the thin films [20,36]. These thin film samples are labelled as C0, C1, C2, C3, C4 and C5.

2.2. Characterization techniques

Structural studies were carried out using X-ray diffractometer (D8 Focus, Bruker, Germany) with Cu Kα source (λ = 1.5408 Å). Surface morphologies of the films were examined using Field Emission Scanning Electron Microscope (FE-SEM) (JSM-6701F, JEOL, JAPAN). Optical properties of the samples were studied using UV–Vis spectrophotometer (JASCO, Japan) in the wavelength range of 350–600 nm. Gas sensing characteristics of the thin films were investigated using a home-made gas sensing set-up described in our previous work [14]. High resistance electrometer (6517 A, Keithley, USA) was used to measure the chemi-resistive behaviour of the developed sensing elements. Sensing studies were carried out at room temperature (302 K) and relative humidity of 54%. The sensing response of the film was calculated using the equation,

$$S = \frac{R_a}{R_g} \quad (1)$$

where, R_a and R_g are the resistance of the sensing element in air and test gas atmosphere respectively.

Table 1
Optimized spray deposition parameters of undoped and Ce-doped ZnO samples.

Parameters	Values
Precursor	Zinc acetate dihydrate (0.1 M) Cerium (III) acetate hydrate (0.002 M, 0.004 M,0.006 M, 0.008 M to 0.01 M)
Solvent	Deionized water
Substrate	Glass
Carrier gas	Compressed air
Compressed air pressure	1 bar
Substrate temperature	523 K
Spray nozzle diameter	0.2 mm
Solution flow rate	2 mL min^{-1}
Spray time	45 s
Spray interval	30 s
Substrate nozzle distance	15 cm
Spray angle	90°

3. Results and discussions

3.1. Structural studies

Fig. 1 shows the XRD patterns of undoped and Ce-doped ZnO thin films. The observed diffraction peaks of the films confirmed the hexagonal polycrystalline wurtzite structure of ZnO and the obtained (100), (002), (101), (102), (110), (103) and (200) crystal plane signatures are in good agreement with the JCPDS card (No. 36-1451). Absence of Ce or CeO_2 peaks in doped samples (C0-C4) revealed the substitution of Ce^{2+} for Zn^{2+} in ZnO lattice in-turn confirmed the dopant concentration in ZnO was below the solubility limit. As the dopant concentration was increased, the peak intensity of undoped ZnO film decreased and this might be due to the degradation of the crystalline quality. But for the C5 sample, a new diffraction peak was observed at 28.7° with (111) orientation, which revealed the formation of CeO_2 crystallites with a face-centered cubic structure and in good agreement with JCPDS card (No. 75-0390). This might be due to the increased concentration of Ce-dopants beyond its solubility limit in ZnO [37].

As expected, a slight shift in the major diffraction peaks was observed due to the influence of Ce-dopants. The observed shift emphasizes the fact that the substituent Ce^{3+}/Ce^{4+} ions with

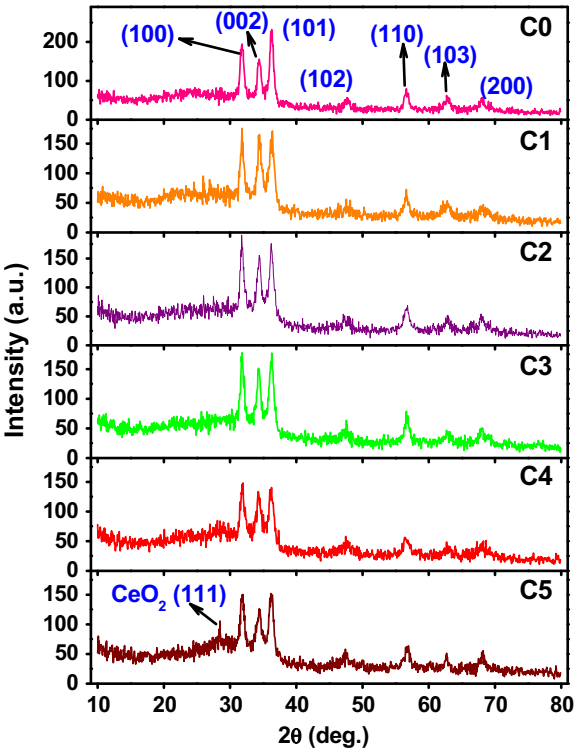

Fig. 1. X-ray diffraction patterns of undoped and Ce-doped ZnO samples.

Table 2
Full width half maximum (FWHM), 2 theta, crystallite size, lattice parameters "c" and "a" and band gap of undoped and Ce-doped ZnO samples.

Sample	FWHM (°)			2 Theta (°)			Crystallite size (nm)			Lattice parameters		Band gap (eV)
	(100)	(002)	(101)	(100)	(002)	(101)	(100)	(002)	(101)	c (Å)	a (Å)	
C0	0.5897	0.5873	0.5725	31.82	34.43	36.28	14	14	15	5.2116	3.2485	3.22
C1	0.7087	0.8017	0.7872	31.82	34.47	36.28	12	10	11	5.2057	3.2485	3.22
C2	0.6224	0.7726	0.7152	31.83	34.41	36.25	13	11	12	5.2145	3.2475	3.23
C3	0.6810	0.7557	0.7296	31.84	34.34	36.24	12	11	11	5.2249	3.2465	3.24
C4	0.9748	1.1213	0.7992	31.89	34.32	36.22	8	7	10	5.2278	3.2416	3.24
C5	0.7955	1.0881	0.6835	31.85	34.39	36.23	10	8	12	5.2175	3.2456	3.26

larger ionic radius of 0.103 nm/0.092 nm than that of Zn^{2+} (0.074 nm) should have distorted the ZnO lattice. Also, the larger ionic radius of Ce^{3+} and Ce^{4+} than Zn^{2+} might have reduced the growth rate of crystallites in-turn degraded the crystalline quality [33,37]. Ce-dopants might have distorted the crystal growth orientation and decreased the crystallite size [38]. This is also evident from the observed lattice parameters (Table 2) and change in the domination of various crystal planes with reference to dopant concentration.

The average crystallite size was calculated using Debye-Scherer's equation,

$$D = \frac{0.9\lambda}{\beta\cos\theta} \quad (2)$$

where, λ is the wavelength of Cu Kα radiation (1.5406 Å), β is the full width at half maximum intensity (FWHM) and θ is the Bragg's diffraction angle. All the observed structural characteristics namely FWHM, 2θ, lattice parameters (a and c) and average

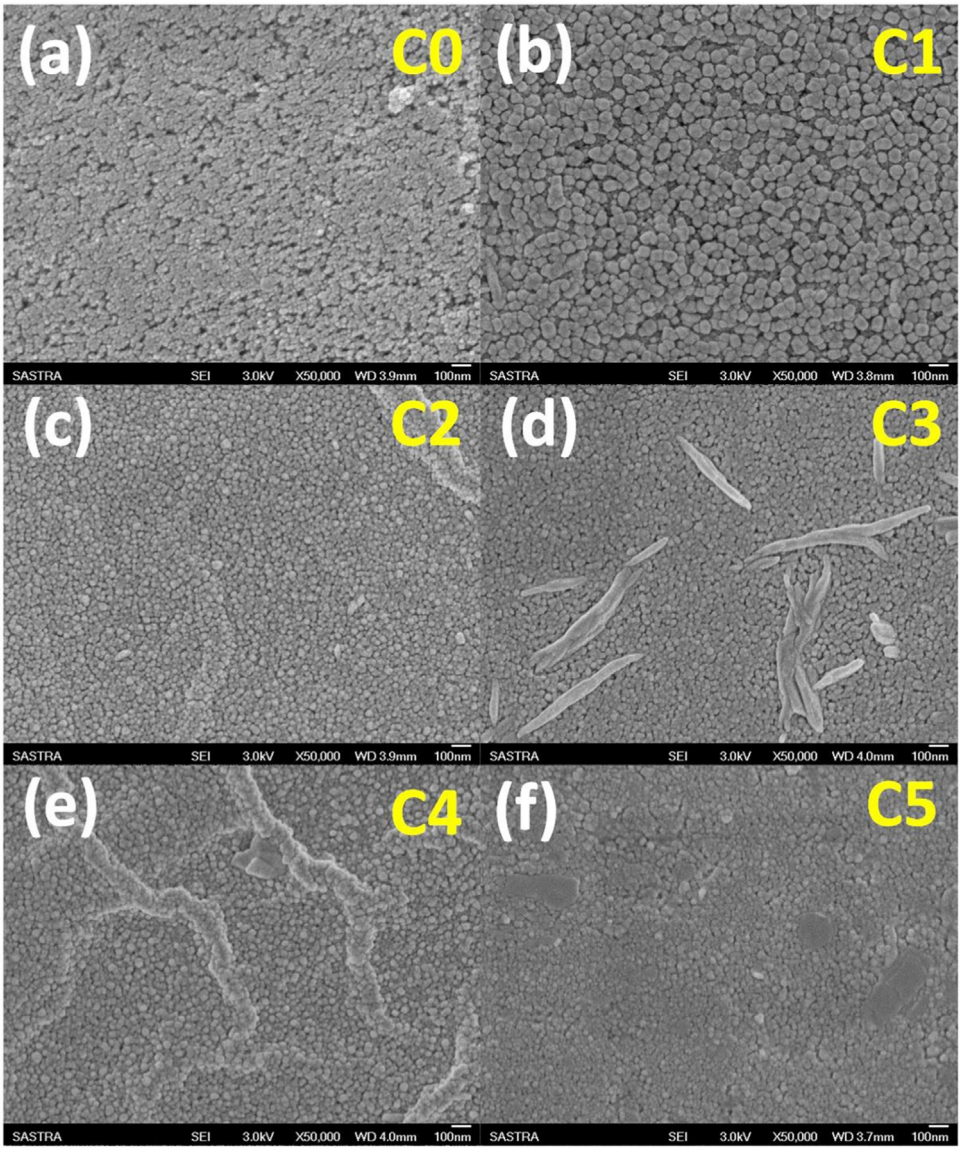

Fig. 2. Scanning electron micrographs of undoped (a) and Ce-doped ZnO (b-f) samples.

crystallite size are presented in Table 2. The average crystallite size was found to be decreased with an increase in Ce-dopant concentration, which is in good agreement with the results observed by Yousefi et al. [31]. This trend might be correlated with the influence of Ce-dopants in the ZnO lattice as well as the observed peak shift in the diffraction pattern.

3.2. Morphological studies

Fig. 2 shows the formation of undoped and Ce-doped ZnO thin films having uniformly distributed spherical grains with differently packed structures and size. It might be due to the influence of Ce-dopant concentrations on the lattice arrangement and grain boundaries. Also, one can observe the decrease in grain size of Ce-doped ZnO thin films with an increase in Ce concentration. The average grain size was found to be decreased from 50 nm to less than 30 nm with an increase in Ce-dopant concentration. A unique spine like nanostructure was appeared on the surface of nano-spherical grains (Fig. 2(C3)) and disappeared for other dopant concentrations. Similar trend was reported for $Zn_{0.9}Ce_{0.1}O$ thin films [37].

3.3. Optical studies

Fig. 3(a) shows the optical transmittance spectra of undoped and Ce-doped ZnO samples. The absorption edges of thin film samples at around 385–395 nm are due to the photoexcitation of electrons from valence to conduction band [39]. The absorption

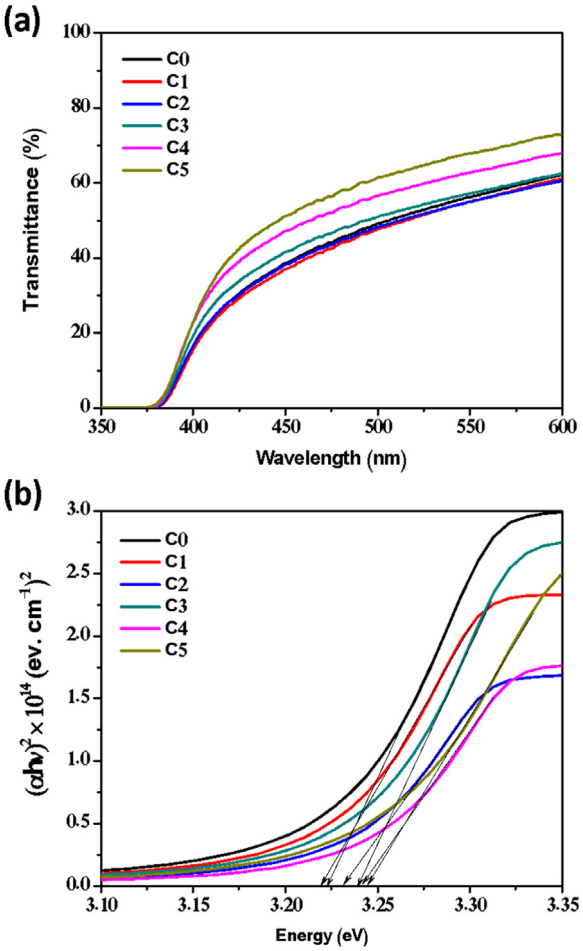

Fig. 3. (a) Transmittance spectra and (b) Tauc's plot of undoped and Ce-doped ZnO samples.

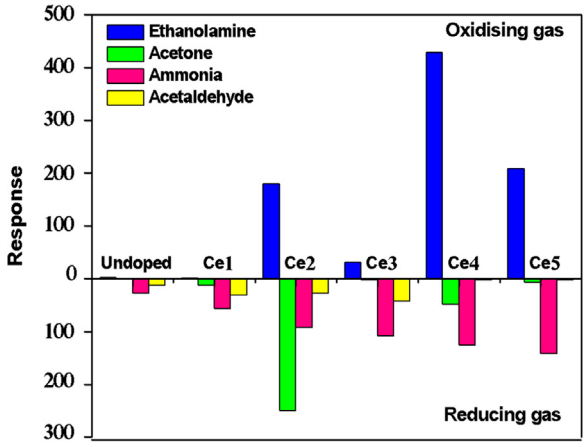

Fig. 4. Sensing response of undoped and Ce-doped ZnO samples towards 100 ppm of ethanolamine, acetone, ammonia and acetaldehyde vapours.

edges were shifted towards the lower wavelengths from 394 to 390 nm as the Ce-dopant concentrations were increased. The observed blue shift might be due to the increased oxygen vacancies, defects in ZnO lattice and disorders in crystallite boundaries as the effect of Ce doping. It also can be correlated with the decrease in the average grain size. The optical band gap was calculated from extrapolating the linear region of plot $(\alpha h\nu)^2$ against photon energy$(h\nu)$ (Fig. 3b). The observed blue shift and band gap widening from 3.2 to 3.26 eV can be explained on the basis of Burstein-Moss effect [37]. The increase in transmittance of thin films from ~55% to 70% also supports the same observation.

3.4. Sensing studies

3.4.1. Selectivity

The undoped and Ce-doped ZnO thin films were exposed to 100 ppm of oxidizing vapour (ethanolamine) and reducing vapours (acetaldehyde, acetone and ammonia) at room temperature and their sensing responses were shown in Fig. 4. Among the six samples, C2 showed a response of 250 towards 100 ppm of acetone (reducing vapour), whereas C4 showed a response of 428 towards 100 ppm of ethanolamine (oxidizing vapour). Both the receptor and transduction functions of C2 and C4 samples were highly selective towards acetone and ethanolamine. The different oxidation states ($Ce^{2+}/Ce^{3+}/Ce^{4+}$) of Ce-dopants in ZnO might have introduced more oxygen vacancies and carrier concentrations in-turn enhanced the sensing response of C2 and C4 samples.

3.4.2. Response and recovery studies

Fig. 5 shows the transient resistance responses of C2 and C4 samples towards 100 ppm of acetone and ethanolamine at room temperature. The observed stable base line resistance at ambient atmosphere after and before interacting with target gas revealed the faster response and recovery characteristics of the sensing elements. The decrease in resistance (Fig. 5(a)) of the sensing element C2 in the presence of acetone vapour confirmed the reducing nature of acetone. At the same time, increase in resistance (Fig. 5(b)) towards ethanolamine revealed the oxidizing nature of ethanolamine vapour. Compared with the available reports, response of the sensing element towards acetone and ethanolamine vapours was found to be better at room temperature (Table 3). The response time of 35 and 20 s and recovery time of 21 and 10 s were observed for C2 and C4 samples towards 100 ppm of acetone and ethanolamine respectively.

3.4.3. Detection limit

The detection efficiency of the sensing elements towards

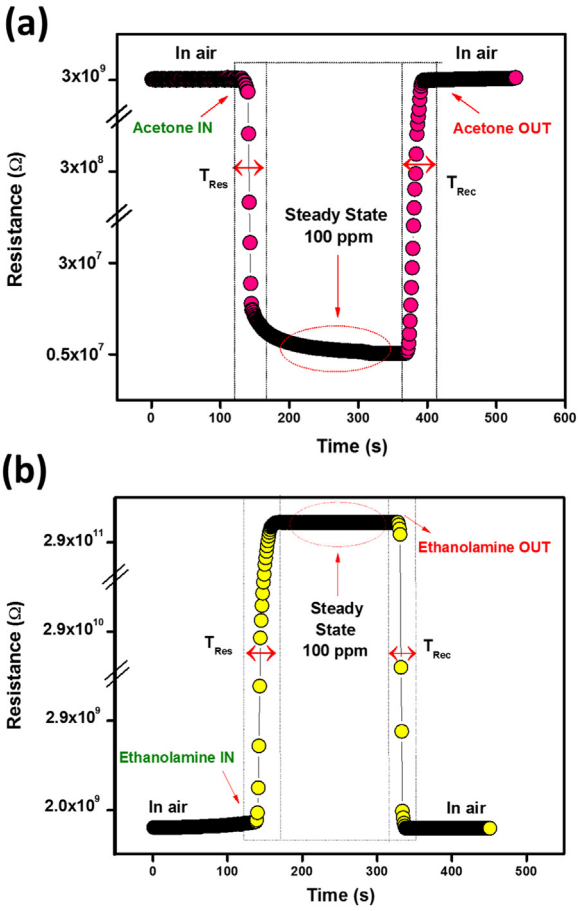

Fig. 5. Transient resistance response of (a) C2 sample towards 100 ppm of acetone and (b) C4 sample towards 100 ppm of ethanolamine at room temperature.

Table 3
Comparison of the responses of various sensor elements towards acetone.

Sample	Concentration (ppm)	Temperature (°C)	Response	Ref.
Ce–ZnO	5	24	3	Present work
ZnO	100	24	73	[18]
SnO_2–RGO	500	24	~7	[27]
Ni–ZnO	100	24	1.61	[28]
TsCuPc–ZnO	50	24	162	[29]
Cr–WO_3	1	Above 24	2.9	[42]
ZnO	500	200	~9.6	[43]
Ce–SnO_2	500	250	33.2	[32]
Ce–SnO_2	500	320	48.5	[33]
Ce–ZnO	100	320	22	[35]
CeO_2–ZnO	500	325	55	[34]
Co–ZnO	100	360	~16	[44]

acetone and ethanolamine was investigated by varying the target vapour concentration from 1 to 500 ppm and is shown in Fig. 6. For 1 ppm and 100 ppm of acetone the obtained response was 3 and 252 for C2 sample. Above 100 ppm, the response was saturated, which might be due to the non-availability of active sites for further gas-solid interaction. Similarly, the response of C4 sample towards ethanolamine from 1 ppm and 500 ppm was 7 and 1850 respectively. Hence, the detection ability of Ce-doped ZnO films (C2 and C4) from 1 ppm to 500 ppm makes them suitable sensors for breath analysis and disease diagnostics.

3.4.4. Sensing mechanism

When the *n*-type semiconducting ZnO thin film was exposed to

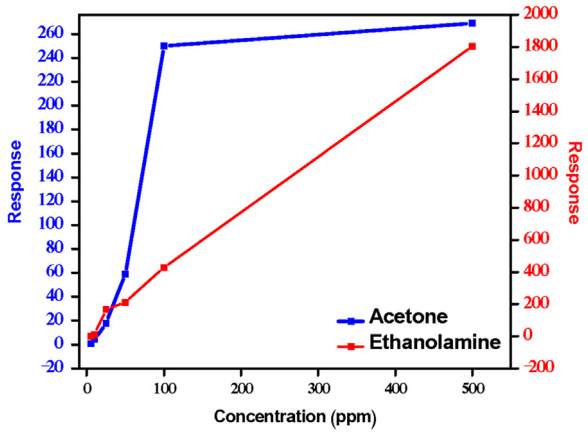

Fig. 6. Sensing responses of C2 and C4 samples towards the various concentrations of acetone and ethanolamine.

the ambient atmosphere, the resistance of the film is increased due to the adsorption of its conduction band electrons by oxygen molecules (Eq. (3)).

$$O_2 + e^-_{(ZnO)} \longrightarrow O^-_{2(ZnO\ surface)} \quad (3)$$

Trapping of electrons from the conduction band lead to increase the width of the space charge region in each grains of the ZnO film in-turn increased the height of the potential barrier [14]. This increased potential barrier or the persuaded resistance is fixed as the base line resistance for all the sensing studies. When the reducing vapours like acetone, ammonia and acetaldehyde were introduced to the Ce-doped ZnO, the resistance decreased from its base line. This trend confirmed the response of the sensor towards reducing gases. The introduced acetone vapour interacted with the adsorbed oxygen ions leading to desorption of the same from the surface. This interaction increased the electron concentration in the conduction band of sensing element as given in Eq. 4 and reduced the height of the potential barrier, thereby enhanced the transduction function and decreased the baseline resistance. The change in resistance of the film has been calculated from the obtained response graph.

$$CH_3COCH_3 + 4O^-_{2(ZnO\ surface)} \longrightarrow 3CO_2\uparrow + 3H_2O\uparrow + 4e^-_{(ZnO\ surface)} \quad (4)$$

When ethanolamine was introduced to the Ce-doped ZnO sensing element (C4), its resistance increased from the base line and attained a steady state Fig. 5(b). The increase in resistance could be due to the oxidizing nature of ethanolamine. Ethanolamine molecules interacted with the adsorbed oxygen to form a bilayer and subsequently it might have reacted with the surface free oxygen molecules (in ambient) to form ammonia, carbon dioxide and water vapour (Eq. 5). Rochelle et al. [40,41] investigated the degradation of ethanolamine in detail and reported that the oxidation of ethanolamine results in the formation of by-products such as ammonia, carbon dioxide, etc. Based on this observation, the sensing mechanism has been proposed as given below:

$$CH_2CH_2OHNH_2 + 2O^-_{2(ZnO\ surface)} \longrightarrow NH_3 + 2CO_2\uparrow + 2H_2O + 2e^-_{(ZnO\ surface)}\uparrow \quad (5)$$

3.4.5. Potential applications

The plethora of gaseous compounds evolved during metabolites act as the best biomarkers, as they can be detected using non-invasive sensors to identify the diseases. As acetone is the signature of type I diabetes, it can be detected quickly with the aid of designed Ce- doped ZnO breath sensor. The sensing efficiency is

high as its response is 3 for 1 ppm of acetone at room temperature. The selectivity of the sensor can be tuned to identify other VOCs like ammonia and acetaldehyde to design a better breath sensor for other diseases.

4. Conclusion

In summary, acetone and ethanolamine sensors using Ce-doped ZnO thin films with varying Ce-dopant concentrations were successfully fabricated. Structural, morphological and optical characteristics cohesively confirmed the influence of Ce-dopants in modulating the grain size and bandgap of ZnO. Among the different Ce-dopant concentrations, films prepared with 0.004 M and 0.008 M of Ce-dopants showed an excellent response towards acetone and ethanolamine vapours respectively with swift response and recovery times. Lower concentration detection of 1 ppm of acetone could be an effective tool to detect type 1 diabetes through exhaled breath analysis. The observed results suggested that the Ce-doped ZnO sensor can be used as a cost effective disease diagnostic tool, which can be used in the fields by the medical field officers as a hand held device for the rapid assessment of the status of the disease.

Acknowledgements

The authors wish to express their sincere thanks to Department of Science & Technology (IDP/IND/2012/41(General) and (SR/FST/ETI-284/2011(C))), Department of Biotechnology (BT/PR10437/PFN/20/779/2013) and Nano Mission Council (SR/NM/PG-16/2007), Government of India. We also wish to acknowledge SASTRA University, Thanjavur for extending infrastructure support to carry out this work.

References

[1] M. Shirasu, K. Touhara, The scent of disease: volatile organic compounds of the human body related to disease and disorder, J. Biochem. 150 (2011) 257–266, http://dx.doi.org/10.1093/jb/mvr090.
[2] W.-H.H. Cheng, W.-J.J. Lee, P. Aghion, J.G.W. Growth, Technology development in breath microanalysis for clinical diagnosis, J. Lab. Clin. Med. 133 (1999) 218–228, http://dx.doi.org/10.1016/S0022-2143(99)90077-X.
[3] M. Corradi, I. Rubinstein, R. Andreoli, P. Manini, A. Caglieri, D. Poli, et al., Aldehydes in exhaled breath condensate of patients with chronic obstructive pulmonary disease, Am. J. Respir. Crit. Care Med. 167 (2003) 1380–1386, http://dx.doi.org/10.1164/rccm.200210-1253OC.
[4] O.B. Crofford, R.E. Mallard, R.E. Winton, N.L. Rogers, J.C. Jackson, U. Keller, Acetone in breath and blood, Trans. Am. Clin. Climatol. Assoc. 88 (1977) 128–139 ⟨http://www.ncbi.nlm.nih.gov/pmc/articles/PMC2441399/⟩.
[5] O.E. Owen, V.E. Trapp, C.L. Skutches, M.A. Mozzoli, R.D. Hoeldtke, G. Boden, et al., Acetone metabolism during diabetic ketoacidosis, Diabetes 31 (1982) 242–248, http://dx.doi.org/10.2337/diabetes.31.3.242.
[6] J. Shin, S.J. Choi, I. Lee, D.Y. Youn, C.O. Park, J.H. Lee, et al., Thin-wall assembled SnO2 fibers functionalized by catalytic Pt nanoparticles and their superior exhaled-breath-sensing properties for the diagnosis of diabetes, Adv. Funct. Mater. 23 (2013) 2357–2367, http://dx.doi.org/10.1002/adfm.201202729.
[7] C.E. Dent, J.M. Walshe, Primary carcinoma of the liver: description of a case with ethanolaminuria, a new and obscure metabolic defect, Br. J. Cancer 7 (1953) 166–180 ⟨http://www.ncbi.nlm.nih.gov/pmc/articles/PMC2007888/⟩.
[8] J. Xu, J. Han, Y. Zhang, Y. Sun, B. Xie, Studies on alcohol sensing mechanism of ZnO based gas sensors, Sens. Actuators B: Chem. 132 (2008) 334–339, http://dx.doi.org/10.1016/j.snb.2008.01.062.
[9] M.J.S.S. Spencer, Gas sensing applications of 1D-nanostructured zinc oxide: Insights from density functional theory calculations, Prog. Mater. Sci. 57 (2012) 437–486, http://dx.doi.org/10.1016/j.pmatsci.2011.06.001.
[10] T. Krishnakumar, R. Jayaprakash, N. Pinna, N. Donato, A. Bonavita, G. Micali, et al., CO gas sensing of ZnO nanostructures synthesized by an assisted microwave wet chemical route, Sens. Actuators B: Chem. 143 (2009) 198–204, http://dx.doi.org/10.1016/j.snb.2009.09.039.
[11] Y.J. Chen, C.L. Zhu, G. Xiao, Ethanol sensing characteristics of ambient temperature sonochemically synthesized ZnO nanotubes, Sens. Actuators B: Chem. 129 (2008) 639–642, http://dx.doi.org/10.1016/j.snb.2007.09.010.
[12] L. Wang, Y. Kang, X. Liu, S. Zhang, W. Huang, S. Wang, ZnO nanorod gas sensor for ethanol detection, Sens. Actuators B: Chem. 162 (2012) 237–243, http://dx.doi.org/10.1016/j.snb.2011.12.073.
[13] J.B.K. Law, J.T.L. Thong, Improving the NH(3) gas sensitivity of ZnO nanowire sensors by reducing the carrier concentration, Nanotechnology 19 (2008) 205502, http://dx.doi.org/10.1088/0957-4484/19/39/399801.
[14] G.K. Mani, J.B.B. Rayappan, A highly selective room temperature ammonia sensor using spray deposited zinc oxide thin film, Sens. Actuators B: Chem. 183 (2013) 459–466, http://dx.doi.org/10.1016/j.snb.2013.03.132.
[15] P. Shankar, J.B.B. Rayappan, Electrospun tailored ZnO nanostructures – role of chloride ions, RSC Adv. 5 (2015) 85363–85372, http://dx.doi.org/10.1039/C5RA15697A.
[16] K. Subbulakshmi, R. Pandeeswari, B.G.G. Jeyaprakash, Surface morphology dependent TMA sensing response of spray deposited ZnO thin films, Superlattices Microstruct. 65 (2014) 219–226, http://dx.doi.org/10.1016/j.spmi.2013.11.002.
[17] D. Ponnusamy, S. Madanagurusamy, Nanostructured ZnO films for room temperature ammonia sensing, J. Electron. Mater. 43 (2014) 3211–3216, http://dx.doi.org/10.1007/s11664-014-3253-8.
[18] V. Elavalagan, P. Shankar, G.K. Mani, J.B.B. Rayappan, A simple and novel room temperature ethanolamine ZnO nanosensor, Nanosci. Nanotechnol. Lett. 6 (2014) 1046–1052, http://dx.doi.org/10.1166/nnl.2014.1881.
[19] F. Fang, J. Futter, A. Markwitz, J. Kennedy, UV and humidity sensing properties of ZnO nanorods prepared by the arc discharge method, Nanotechnology 20 (2009) 245502, http://dx.doi.org/10.1088/0957–4484/20/24/245502.
[20] G.K. Mani, J.B.B. Rayappan, A highly selective and wide range ammonia sensor—Nanostructured ZnO:Co thin film, Mater. Sci. Eng. B 191 (2015) 41–50, http://dx.doi.org/10.1016/j.mseb.2014.10.007.
[21] L. Krishnakumar, K. Gnanasekaran, M. Elayaperumal, G.K. Mani, K. K, J.B. B. Rayappan, et al., Effective ammonia detection using n-ZnO/p-NiO heterostructured nanofibers, IEEE Sens. J. (2016), http://dx.doi.org/10.1109/JSEN.2016.2517085.
[22] G.K. Mani, J.B.B. Rayappan, Influence of copper doping on structural, optical and sensing properties of spray deposited zinc oxide thin films, J. Alloy. Compd. 582 (2014) 414–419, http://dx.doi.org/10.1016/j.jallcom.2013.07.146.
[23] A.J. Kulandaisamy, C. Karthek, P. Shankar, G.K. Mani, J.B.B. Rayappan, Tuning selectivity through cobalt doping in spray pyrolysis deposited ZnO thin films, Ceram. Int. 42 (2016) 1408–1415, http://dx.doi.org/10.1016/j.ceramint.2015.09.084.
[24] F. Fang, J. Kennedy, J. Futter, T. Hopf, A. Markwitz, E. Manikandan, et al., Size-controlled synthesis and gas sensing application of tungsten oxide nanostructures produced by arc discharge, Nanotechnology 22 (2011) 335702, http://dx.doi.org/10.1088/0957-4484/22/33/335702.
[25] F. Paraguay D, M. Miki-Yoshida, J. Morales, J. Solis, W. Estrada L, Influence of Al, In, Cu, Fe and Sn dopants on the response of thin film ZnO gas sensor to ethanol vapour, Thin Solid Films 373 (2000) 137–140, http://dx.doi.org/10.1016/S0040-6090(00)01120-2.
[26] J. Kennedy, P.P. Murmu, E. Manikandan, S.Y. Lee, Investigation of structural and photoluminescence properties of gas and metal ions doped zinc oxide single crystals, J. Alloy. Compd. 616 (2014) 614–617, http://dx.doi.org/10.1016/j.jallcom.2014.07.179.
[27] D. Zhang, A. Liu, H. Chang, B. Xia, Room-temperature high-performance acetone gas sensor based on hydrothermal synthesized SnO_2-reduced graphene oxide hybrid composite, RSC Adv. 5 (2015) 3016–3022, http://dx.doi.org/10.1039/C4RA10942B.
[28] H. Ahn, Y. Wang, S. Hyun Jee, M. Park, Y.S. Yoon, D.J. Kim, Enhanced UV activation of electrochemically doped Ni in ZnO nanorods for room temperature acetone sensing, Chem. Phys. Lett. 511 (2011) 331–335, http://dx.doi.org/10.1016/j.cplett.2011.06.045.
[29] A.K. Bal, Room-temperature acetone sensing by sulfonated copper phthalocyanine (TsCuPc)-modified ZnO films, J. Electron. Mater. 44 (2014) 144–151, http://dx.doi.org/10.1007/s11664-014-3461-2.
[30] N. Skorodumova, R. Ahuja, S. Simak, I. Abrikosov, B. Johansson, B. Lundqvist, Electronic, bonding, and optical properties of CeO_2 and Ce_2O_3 from first principles, Phys. Rev. B 64 (2001) 115108, http://dx.doi.org/10.1103/PhysRevB.64.115108.
[31] M. Yousefi, R. Azimirad, M. Amiri, A.Z. Moshfegh, Effect of annealing temperature on growth of Ce-ZnO nanocomposite thin films: X-ray photoelectron spectroscopy study, Thin Solid Films 520 (2011) 721–725, http://dx.doi.org/10.1016/j.tsf.2011.06.081.
[32] P. Song, Q. Wang, Z. Yang, Preparation, characterization and acetone sensing properties of Ce-doped SnO_2 hollow spheres, Sens. Actuators B: Chem. 173 (2012) 839–846, http://dx.doi.org/10.1016/j.snb.2012.07.115.
[33] D. Liu, T. Liu, H. Zhang, C. Lv, W. Zeng, J. Zhang, Gas sensing mechanism and properties of Ce-doped SnO_2 sensors for volatile organic compounds, Mater. Sci. Semicond. Process. 15 (2012) 438–444, http://dx.doi.org/10.1016/j.mssp.2012.02.015.
[34] A.V. Rajgure, N.L. Tarwal, J.Y. Patil, L.P. Chikhale, R.C. Pawar, C.S. Lee, et al., Gas sensing performance of hydrothermally grown CeO_2–ZnO composites, Ceram. Int. 40 (2014) 5837–5842, http://dx.doi.org/10.1016/j.ceramint.2013.11.025.
[35] C. Ge, C. Xie, S. Cai, Preparation and gas-sensing properties of Ce-doped ZnO thin-film sensors by dip-coating, Mater. Sci. Eng. B: Solid-State Mater. Adv. Technol. 137 (2007) 53–58, http://dx.doi.org/10.1016/j.mseb.2006.10.006.
[36] I. Muniyandi, G.K. Mani, P. Shankar, J.B.B. Rayappan, Effect of nickel doping on structural, optical, electrical and ethanol sensing properties of spray deposited nanostructured ZnO thin films, Ceram. Int. 40 (2014) 7993–8001, http://dx.doi.

org/10.1016/j.ceramint.2013.12.150.
[37] S. Muthu Kumaran, R. Gopalakrishnan, Structural, optical and photoluminescence properties of $Zn_{1-x}Ce_xO$ (x=0, 0.05 and 0.1) nanoparticles by sol–gel method annealed under Ar atmosphere, J. Sol-Gel Sci. Technol. 62 (2012) 193–200, http://dx.doi.org/10.1007/s10971-012-2708-8.
[38] G.K. Mani, J.B.B. Rayappan, ZnO nanoarchitectures: Ultrahigh sensitive room temperature acetaldehyde sensor, Sens. Actuators B: Chem. 223 (2016) 343–351, http://dx.doi.org/10.1016/j.snb.2015.09.103.
[39] J. Kennedy, P.P. Murmu, J. Leveneur, A. Markwitz, J. Futter, Controlling preferred orientation and electrical conductivity of zinc oxide thin films by post growth annealing treatment, Appl. Surf. Sci. 367 (2016) 52–58, http://dx.doi.org/10.1016/j.apsusc.2016.01.160.
[40] A.J. Sexton, G.T. Rochelle, Reaction products from the oxidative degradation of monoethanolamine, Ind. Eng. Chem. Res. 50 (2011) 667–673, http://dx.doi.org/10.1021/ie901053s.
[41] G.S. Goff, G.T. Rochelle, Monoethanolamine degradation: O_2 mass transfer effects under CO_2 capture conditions, Ind. Eng. Chem. Res. 43 (2004) 6400–6408, http://dx.doi.org/10.1021/ie0400245.
[42] L. Wang, K. Kalyanasundaram, M. Stanacevic, P. Gouma, Nanosensor device for breath acetone detection, Sens. Lett. 8 (2010) 709–712, http://dx.doi.org/10.1166/sl.2010.1334.
[43] N. Kakati, S.H. Jee, S.H. Kim, J.Y. Oh, Y.S. Yoon, Thickness dependency of sol-gel derived ZnO thin films on gas sensing behaviors, Thin Solid Films 519 (2010) 494–498, http://dx.doi.org/10.1016/j.tsf.2010.08.005.
[44] L. Liu, S. Li, J. Zhuang, L. Wang, J. Zhang, H. Li, et al., Improved selective acetone sensing properties of Co-doped ZnO nanofibers by electrospinning, Sens. Actuators B: Chem. 155 (2011) 782–788, http://dx.doi.org/10.1016/j.snb.2011.01.047.